Journal of ELECTRONIC MATERIALS, Vol. 50, No. 4, 2021
https://doi.org/10.1007/s11664-021-08752-8
© 2021 The Minerals, Metals & Materials Society

ORIGINAL RESEARCH ARTICLE

Influence of As^+ Ion Implantation on Properties of MBE HgCdTe Near-Surface Layer Characterized by Metal–Insulator–Semiconductor Techniques

A.V. VOITSEKHOVSKII,[1] S.N. NESMELOV ,[1,3] S.M. DZYADUKH,[1] V.S. VARAVIN,[2] S.A. DVORETSKY,[1,2] N.N. MIKHAILOV,[2] G.Y. SIDOROV,[2] M.V. YAKUSHEV,[2] and D.V. MARIN[2]

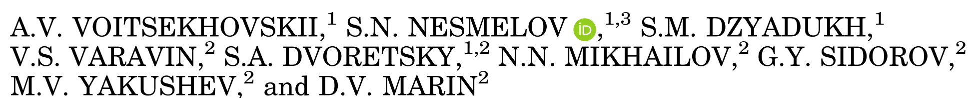

1.—National Research Tomsk State University, 36 Lenina Ave., 634050 Tomsk, Russia. 2.—Rzhanov Institute of Semiconductor Physics SB RAS, 13 Lavrentiev Ave., 630090 Novosibirsk, Russia. 3.—e-mail: nesm69@mail.ru

The effect of As^+ ion implantation on the electrical properties of the near-surface layer of *n*-HgCdTe films grown by molecular beam epitaxy (MBE) on Si (310) substrates was experimentally studied. A specific feature of MBE *n*-$Hg_{0.78}Cd_{0.22}Te$ films is the presence of near-surface graded-gap layers with a high CdTe content, formed during epitaxial growth. The properties of as-grown films and films after As^+ ion implantation with ion energy of 200 keV and fluence of 10^{14} cm^{-2} were studied. Post-implantation activation annealing was not performed. Test metal–insulator–semiconductor (MIS) structures were created based on as-grown and as-implanted samples by plasma-enhanced atomic layer deposition of Al_2O_3 insulator films. The admittance of the fabricated MIS structures was measured over a wide range of frequencies and temperatures. When determining the parameters of MIS structures, we used techniques that take into account the presence of near-surface graded-gap layers and series resistance of the HgCdTe film bulk, as well as the high density of slow surface states. It was found that, in as-implanted samples, the donor center concentration in the near-surface layer exceeds 10^{17} cm^{-3} and increases with distance from the HgCdTe-Al_2O_3 interface (at least up to 90 nm). After implantation, the conductivity of MBE HgCdTe film bulk increases markedly. It was shown that, for as-implanted samples, the generation rate of minority charge carriers in the MBE HgCdTe surface layer is significantly reduced, which indicates the appearance of a low defect layer with a thickness of at least 90 nm.

Key words: Mercury cadmium telluride, molecular beam epitaxy, graded-gap layer, ion implantation, MIS structure, admittance

INTRODUCTION

The semiconductor solid solution of mercury cadmium telluride ($Hg_{1-x}Cd_xTe$, HgCdTe) has long been used to create highly sensitive infrared detectors.[1,2] The energy gap of $Hg_{1-x}Cd_xTe$ depends on the CdTe content, which allows the creation of infrared detectors with interband absorption (intrinsic detectors) for various spectral regions, including MWIR (3–5 μm) and LWIR (8–14 μm). New opportunities for the HgCdTe-based detector development have arisen as a result of the progress of epitaxial methods, such as molecular beam epitaxy (MBE)[3] and metalorganic chemical vapor deposition.[4] The most common type of detectors based on MBE HgCdTe are hybrid photodiode

(Received June 16, 2020; accepted January 13, 2021; published online February 2, 2021)

arrays,[5–9] in which the *pn* junction is created by ion implantation and subsequent thermal annealing. Currently, As^+ ion implantation is widely used, which was first proposed as a method for creating *p*-on-*n* junctions in HgCdTe photodiodes more than 40 years ago.[10,11] To improve the technology for creating *pn* photodiodes based on MBE HgCdTe, significant research efforts have been directed to the study of post-implantation material properties, including the mechanisms of the radiation defect evolution. The properties of HgCdTe films after ion implantation were studied using Hall and optical measurements, Rutherford backscattering, and electron microscopy.[12–17] An important task is also to study the processes occurring in HgCdTe films after post-implantation annealing.[18–20] A complete understanding of all the features of the processes during ion implantation in MBE HgCdTe in the case of the presence of surface graded-gap layers, which are used to reduce the effect of surface recombination on the properties of photodiodes,[21] has not yet been achieved.

Metal–insulator–semiconductor (MIS) structures are a convenient tool for studying the properties of the surface layers of semiconductors and the interface between dielectric and semiconductor layers.[22–24] In studies of the post-implantation properties of MBE HgCdTe films with graded-gap layers, such MIS techniques have recently been applied.[25,26] The use of MIS measurements in studies of the properties of graded-gap MBE HgCdTe films became possible after the development of a number of techniques,[27–29] that take into account the presence of graded-gap layers and make it possible to exclude the effect of the recharging of slow surface states on the measurement results. In studies of the admittance of MIS structures, one can obtain information about the properties of the surface layer of a semiconductor. The thickness of this layer is determined by the depth of penetration of the electric field into the semiconductor. Therefore, the results of MIS measurements can supply the data on the electrical properties of HgCdTe films obtained using the Hall method.

This paper presents the results of studies of the effect of As^+ ion implantation on the electrical properties of MBE *n*-HgCdTe films obtained by measuring the admittance of test MIS structures in wide ranges of frequencies, voltages, and temperatures. Two MBE *n*-HgCdTe films with the composition in the operating layer of 0.22 and close parameters of the graded-gap layers were chosen for studies. MIS structures were created by depositing Al_2O_3 dielectric layers on top of as-grown MBE HgCdTe films, as well as films after implantation (as-implanted films). Post-implantation activation annealing was not performed for the as-implanted samples (the modes of such annealing are described, for example, in Ref. 26). The experimental data were processed using specially developed techniques to determine the most important parameters of the MIS structures based on MBE HgCdTe with near-surface graded-gap layers.

EXPERIMENTAL PROCEDURES

The *n*-HgCdTe films were grown at the Rzhanov Institute of Semiconductor Physics of the Siberian Branch of the Russian Academy of Sciences by MBE on Si (310) substrates.[30] ZnTe (50 nm) and CdTe (5 μm) buffer layers were deposited on top of the silicon substrate. Two heteroepitaxial *n*-$Hg_{1-x}Cd_xTe$ films (samples A and B) were grown. The composition in the operating layer for both films was close to 0.22. The films were doped with an indium impurity during epitaxial growth. Graded-gap layers with increased composition *x* were created on both sides of the working layers. The growth of $Hg_{1-x}Cd_xTe$ for samples A and B films began with compositions of 0.28 and 0.265, respectively. In the range of coordinates from 0 μm to 0.7 μm, the composition remained constant, since growth conditions were kept constant. Further, the composition deliberately changed due to a change in the tellurium flux at unchanged fluxes of cadmium and mercury and the temperature of the substrate. The parameters of the upper graded-gap layers for films A and B were close. For sample A, the composition on the surface reached 0.451, while for sample B it was 0.453. The thickness of the upper graded-gap layer for both films was about 400 nm. The distribution of the composition over the thickness of the films was monitored during the growth process using an automatic ellipsometer (Fig. 1).

After growth, each of the films (samples A and B) was divided into two parts. One of the parts was not exposed to external influences (as-grown samples), and ion implantation was applied to the other part (as-implanted samples). Ion implantation was carried out using the IMC200 setup. The energy of As^+ ions was 200 keV, and fluence was 10^{14} cm^{-2}. For both types of samples (samples A and B), the projected As ion range for this regime was about 93 nm, and the total range was close to 350 nm.[15]

To study the properties of the surface layer of the as-grown and as-implanted HgCdTe films, test MIS

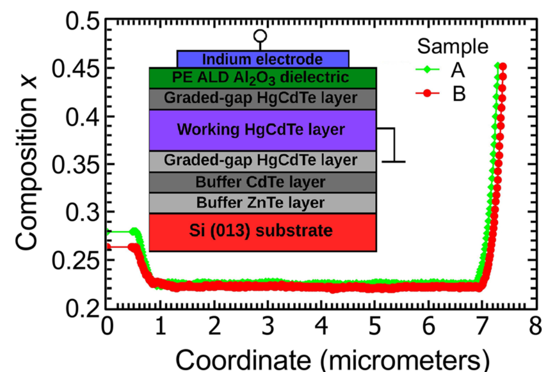

Fig. 1. Composition profiles for samples A and B obtained using ellipsometry. The inset shows the layer layout in the test MIS structure.

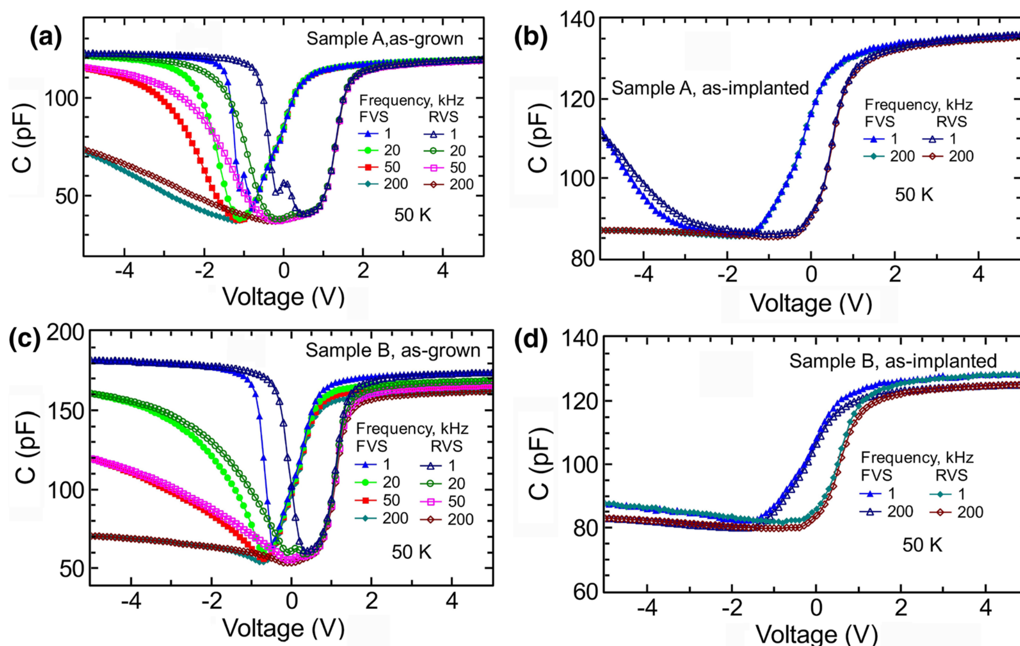

Fig. 2. *CV* characteristics for as-grown (a, c) and as-implanted (b, d) samples A (a, b) and B (c, d), measured at different frequencies at 50 K for FVS and RVS.

structures were created with about 90-nm-thick Al_2O_3 dielectric formed using plasma-enhanced atomic layer deposition (PE ALD).[31–34] This PE ALD Al_2O_3 dielectric was deposited directly onto the surface of the HgCdTe film without using a photoresist. The temperature during the deposition of the dielectric Al_2O_3 layers did not exceed 120°C, to prevent mercury from leaving the surface layer of HgCdTe. Frontal indium electrodes were formed on top of the PE ALD Al_2O_3 dielectric by thermal evaporation at low temperatures (< 100°C). This backward indium electrode was formed by thermal evaporation in vacuum after etching the graded-gap HgCdTe layer in a solution of bromine–methanol. The location of the layers in the fabricated test MIS structures is shown in the inset in Fig. 1.

The admittance of the test MIS structures was measured using an automated setup. The main elements of this setup are a non-optical Janis cryostat, LakeShore controller and Agilent E4980A immittance meter. Admittance measurements were carried out over wide ranges of temperatures (from 8 K to 300 K) and frequencies (from 1 kHz to 2000 kHz). The forward direction of the voltage sweep (FVS) was the change in the bias voltage from negative values to positive ones. For the reverse direction of the voltage sweep (RVS), the bias voltage was changed from positive values to negative ones.

The procedures for processing the results of admittance measurements, as well as the equivalent circuits of MIS devices under various modes, have been previously described in detail.[35,36] The values of the dielectric capacitance (C_{ins}) and the resistance of the epitaxial film bulk (R_{bulk}) were determined from the results of measurements of the admittance of MIS structures in the accumulation mode. Knowing the values of C_{ins} and R_{bulk}, the values of the capacitance and differential resistance of the near-surface semiconductor layer can be found from the results of measuring the admittance at various bias voltages.[37] Then, the values of the admittance of the MIS structure can be found with the exclusion of the effect of the resistance of the epitaxial film bulk using expressions from.[35–37]

The structures under study have a number of specific features (the presence of near-surface graded-gap layers in semiconductor layer[36,38] and high density of slow surface states at the interface between the dielectric and semiconductor layers[39,40]). These peculiarities do not allow using the classical MIS techniques[22] unchanged. The high-frequency behavior of *CV* curves for MIS structures based on $Hg_{1-x}Cd_xTe$ (x = 0.21–0.23) is observed at frequencies exceeding several MHz, which complicates the determination of the dopant concentration in the near-surface semiconductor layer from the high-frequency capacitance value in the strong inversion mode.[22] Therefore, to determine the donor concentration in the HgCdTe surface layer, we used another method, which was specially developed for studying MIS structures based on graded-gap HgCdTe.[27,28,38] It was shown earlier that *CV* curves of MIS structures based on MBE HgCdTe with near-surface graded-gap layers can have a low-frequency behavior with respect to the recharge time of the inversion layer, but, in a wide range of conditions, they have a high-frequency behavior with respect to the recharge time of surface states.[27,28] In this case, it is possible to determine the donor concentration

in the surface HgCdTe layer by the capacitance value in the minimum of the *CV* curve, since the surface states do not have time to recharge and do not contribute to the minimum capacitance value. The value of the donor concentration in the surface HgCdTe layer was determined by comparing the experimental curve and the ideal curve calculated by numerically solving the Poisson equation taking into account changes in the composition in the graded-gap layer.[28,38]

From this value of the donor concentration in the near-surface layer of the HgCdTe film, one can calculate the value of the flat band capacitance and determine the values of the flat band voltage for FVS and RVS.[22,41] The density of slow surface states was estimated from the magnitude of the flat band voltage shift for FVS and RVS.[22,34] The value of the differential resistance of the space charge region (SCR) in the strong inversion mode (R_{SCR}) is inversely proportional to the generation rate of minority charge carriers in the near-surface semiconductor layer, and can be found from admittance measurements using simple formulae.[35,36] When plotting the dependences of the donor concentration on the coordinate in the near-surface semiconductor layer from the slope of the *CV* curve in the depletion mode,[42] we used a technique for measuring electrical characteristics with a complex voltage sweep shape,[43] which makes it possible to exclude the effect of recharge of slow surface states on the measurement results. The effectiveness of this technique has been previously shown in studies of the properties of MIS structures based on HgCdTe with graded-gap layers.[24,29] It can be noted that the implementation of the depletion approximation is only necessary when determining the dependence of the donor concentration on the coordinate by the slope of the *CV* characteristic.[42] In cases of determining other parameters of the MIS structures, this approximation is not required.

RESULTS AND DISCUSSION

Figure 2 shows the *CV* characteristics of test MIS structures based on films A and B (as-grown and as-implanted), measured at various frequencies at the temperature of 50 K for FVS and RVS. It can be seen from Fig. 2a and c that the *CV* curves for the as-grown samples show an almost low-frequency behavior at the frequency of 1 kHz. The low-frequency behavior of the *CV* curves of MIS structures based on an *n*-type semiconductor is observed if the hole concentration in the inversion layer manages to follow changes in the ac test voltage.[22,41] Then, the capacitance of the MIS structure in the strong inversion mode is close to the capacitance of the dielectric layer (and the capacitance of the MIS structure in the accumulation mode), since the capacitance of the inversion layer is large. In cases of high-frequency *CV* behavior, the concentration in the inversion layer characteristic does not have time to noticeably change with a change in the test voltage. In this case, the capacitance of the MIS structure in the strong inversion mode takes a minimum value, which depends on the donor concentration and dielectric parameters.[22,41]

The *CV* characteristics of the as-grown samples have hysteresis associated with the recharging of slow surface states located near the interface between the semiconductor and the dielectric layers.[39,40] Such hysteresis is characteristic of MIS structures based on MBE HgCdTe with near-surface graded-gap layers when using PE ALD Al_2O_3 as a dielectric.[39,40] From Fig. 2b and d, it can be seen that the *CV* characteristics of MIS structures based on MBE HgCdTe films after implantation show a higher-frequency behavior. For these structures, the curves at 1 kHz exhibit near-high-frequency behavior. The high-frequency behavior of the *CV* characteristics is realized if the generation rate of minority charge carriers in the space charge region is insufficient for the carrier concentration in the inversion layer to follow changes in the ac test voltage.[22,41] For clarity, capacitance dependences at the frequencies of 20 kHz and 50 kHz are not shown in Fig. 2b and d, since *CV* characteristics at the frequencies of 1 kHz and 200 kHz are quite close. For the as-implanted samples, the hysteresis of the *CV* curves slightly decreases. For the as-grown samples A and B, the dopant concentration in the surface layer turned out to be 4.6×10^{15} cm^{-3} and 3.9×10^{15} cm^{-3}, respectively, which is in good agreement with the technologically specified values of indium concentration. For the as-implanted samples A and B, the donor concentration in the surface layer increased significantly and amounted to 9.7×10^{16} cm^{-3} and 1.04×10^{17} cm^{-3}, respectively. This increase is associated with the formation of donor-type defects during implantation. In Refs. 44, 45, it was shown that, after implantation, two types of spatially separated donor-type radiation structural defects in the radiation-damaged region appear. It is most likely that the nature of the two types of donor radiation defects is associated with radiation structurally extended and quasi-point defects that have captured interstitial mercury. It should be recalled that post-implantation annealing to activate the acceptor As impurity was not performed for the studied as-implanted samples.

Figure 3a and b shows the temperature dependences of the MIS capacitance for samples A and B, respectively, measured in the accumulation and strong inversion modes at the frequency of 100 kHz. It can be seen that the capacitance in the accumulation mode is relatively weakly dependent on temperature. The capacitance in the strong inversion mode increases with temperature, which is associated with the transition of *CV* curves from high-frequency to low-frequency behavior with an increase in the generation rate of minority charge carriers (holes). For the as-grown samples, the transition to low-frequency behavior occurs at much

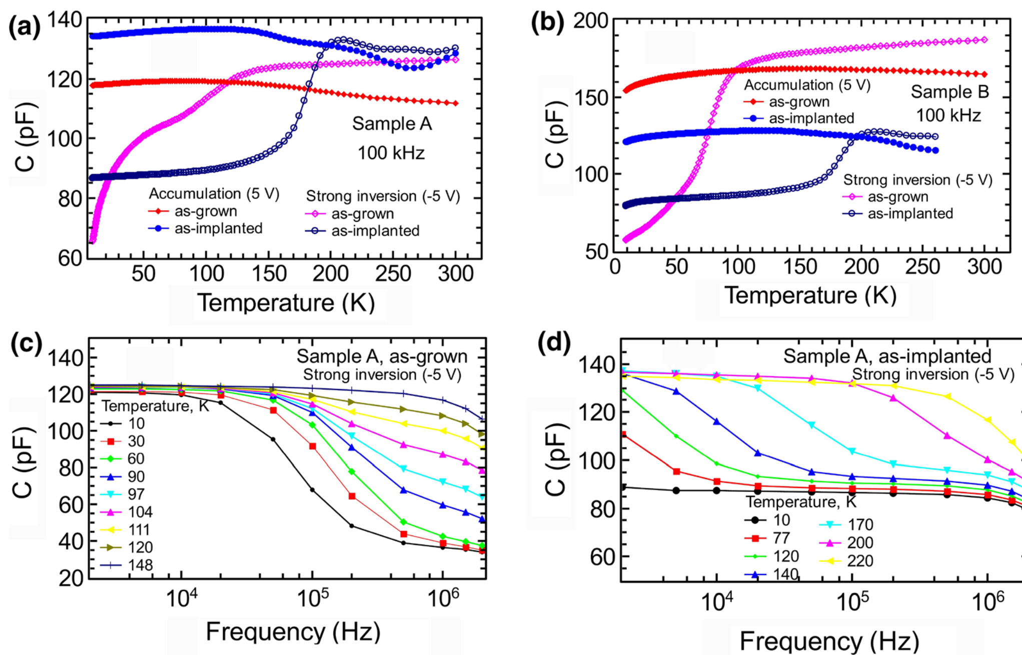

Fig. 3. Temperature dependences of the capacitance for as-grown and as-implanted samples A (a) and B (b) at 100 kHz and various voltages, and frequency dependences of the capacitance in the strong inversion mode for as-grown (c) and as-implanted (d) samples A measured at different temperatures.

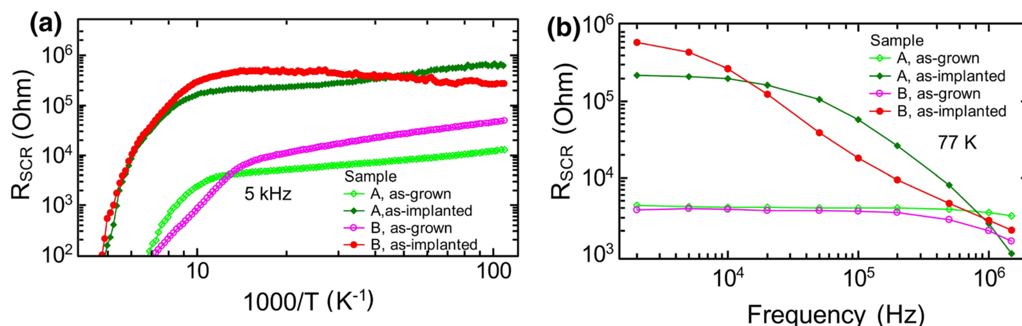

Fig. 4. Temperature dependences of the differential resistance of the space-charge region for samples A and B measured in the strong inversion mode (– 5 V) at 5 kHz (a). Frequency R_{SCR} dependences for samples A and B at 77 K (b)

lower temperatures than for the as-implanted samples. Figure 3c and d shows the frequency dependences of the capacitance in the strong inversion mode measured at different temperatures for as-grown and as-implanted samples A. It can be seen that, for the as-grown samples, the transition to the high-frequency behavior occurs at higher frequencies, which indicates a higher generation rate of minority charge carriers (holes) in this sample.

Figure 4a shows the temperature dependences of the R_{SCR} in the strong inversion mode, measured for as-grown and as-implanted samples at the frequency of 5 kHz. It can be seen that the R_{SCR} values are much higher for the as-implanted samples, which indicates a lower generation rate of minority charge carriers. The decrease in the generation rate is possible due to a lower defect concentration in the surface HgCdTe layer after ion implantation. The change in the defective system of the surface HgCdTe layer after implantation is confirmed by the change in the form of the R_{SCR} frequency dependences measured at the temperature of 77 K (Fig. 4b).

It can be noted that the use of MIS measurements made it possible to clearly demonstrate the appearance of a thin surface layer with a low defect density after implantation. The existence of this layer was first established in Ref. 11 and later confirmed using bright-field transmission electron microscopy[15,16,25] and high-resolution transmission electron microscopy.[25] The formation of such a layer may be associated with a recombination of radiation defects that occurs during implantation itself. It was previously noted that the appearance of this layer is

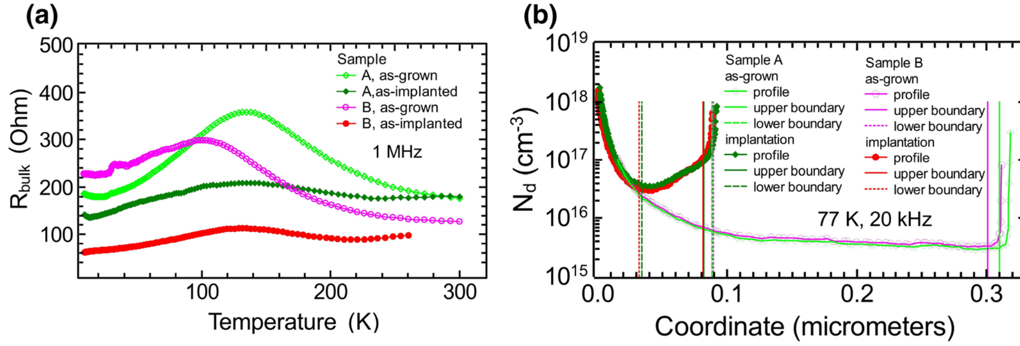

Fig. 5. Temperature dependences of the series resistance of the epitaxial film bulk for the as-grown and as-implanted samples A and B measured at 1 MHz (a). Coordinate dependences of the donor concentration for as-grown and as-implanted samples A and B constructed using the "narrow swing" technique (b).

characteristic of materials with a strong ionic nature of chemical bonds.[13]

Figure 5a shows the temperature dependences of the series resistance of the R_{bulk} for the as-grown and as-implanted samples A and B. It can be seen that the R_{bulk} values are much lower for the as-implanted samples, which indicates an increase in the conductivity of the MBE HgCdTe film bulk. This effect may occur due to changes in both the concentration and mobility of charge carriers. Significant hysteresis does not allow calculating the dependence of the donor concentration directly from the *CV* characteristics of MIS structures based on MBE HgCdTe with graded-gap layers according to the procedure described in Ref. 44. Therefore, to calculate the concentration profiles, we used the measurements of the first derivative of the capacitance using the "narrow swing" method, which was first proposed for the study of InSb-based MIS structures,[43] and later was successfully used for the investigation of MIS structures based on MBE HgCdTe.[24,29] Figure 5b shows the distribution of donor concentration over thickness plotted for the as-grown and as-implanted samples A and B. It is seen that an almost uniform distribution of the concentration of indium impurity is observed for the as-grown samples. The values of concentration are in good agreement with the technologically specified values, as well as with the values found from the minimum of *CV* characteristics. After implantation, the donor concentration increases with the distance from the interface with the dielectric. At a depth of about 90 nm, it is about 10^{17} cm^{-3}, which is in good agreement with the values found from the minimum of the *CV* curves. The technique for determining the donor profile from the slope of the *CV* curve[42] is effective only when the depletion approximation is fulfilled. That means that the screening of the external electric field in the near-surface layer is achieved due to the charge of immobile ionized impurities, and is not due to the charge of the layers of mobile charge carriers, which play an important role in the accumulation and inversion modes. Expressions for the boundaries of the coordinate range, where the error in determining the donor concentration does not exceed 5%, for the MIS structure based on a semiconductor with uniform distribution of the composition and donor concentration are given in Ref. 46. It was previously shown that, in the presence of a graded-gap layer, it is possible to determine the dopant concentration in a wider range of coordinates.[29] The lower and upper boundaries of the range have been calculated for the studied MIS structures based on HgCdTe with near-surface graded-gap layers. In Fig. 5b, solid vertical lines show the upper boundaries of the valid ranges for determining the donor center concentration, and the dashed lines show the lower boundaries of the valid ranges. The decrease in the upper limit of the coordinate range for the as-implanted samples can be qualitatively explained by the fact that the maximum width of the SCR, which is realized in the strong inversion mode, decreases with an increase in the donor concentration.[22,41] Despite the limited range of coordinates within which the donor concentration can be found, the upper limit of the range for the as-implanted samples is close to the value of the projected ion range (93 nm). It can be noted that, at low fluence values, the maximum donor center concentration after implantation is observed at the depth of the projected range. From Fig. 5b, it follows that the thickness of the surface layer with low defect density in the as-implanted samples is at least 90 nm, which slightly exceeds the values of 40–50 nm[15,16,25] and 70 nm[47] found using transmission electron microscopy.

Table I shows the values of the main parameters of the MIS structures, determined from the measurements of admittance at the temperature of 77 K. The density of slow surface states (N_{ss}) was determined by the shift of *CV* curves for RVS and FVS at flat band voltages. The flat band capacitance values were found using the formulae from Ref. 17 using the donor concentration (N_d) values found from the minimum of *CV* curves. Resistance values (R_{SCR} and R_{bulk}) were found from the admittance

Table I. Parameters of MIS structures determined at 77 K

Sample	N_{ss}, cm^{-2}	N_d, cm^{-3}	R_{SCR}, kΩ	R_{bulk}, Ω
A, as-grown	6.12×10^{11}	4.6×10^{15}	4.1	258
A, after implantation	3.52×10^{11}	9.7×10^{16}	212.9	185
B, as-grown	4.72×10^{11}	3.9×10^{15}	3.7	282
B, after implantation	3.57×10^{11}	1.0×10^{17}	436.1	90

measurements at the frequencies of 5 kHz and 1000 kHz, respectively.

From Table I, it follows that the as-implanted samples A and B have lower values of the density of slow states (by 25–50%), large values of the donor concentration in the surface layer (about 10^{17} cm^{-3}), higher values of the differential resistance of the SCR (50–100 times higher), and lower values of the series bulk resistance R_{bulk} (30–60% lower) in comparison with the as-grown samples. It can be noted that the MIS measurements are most informative when studying the properties of a thin near-surface MBE HgCdTe layer, in which a significant decrease in the generation rate of minority charge carriers and an increase in the donor concentration after implantation were observed. For a more detailed study of changes in the properties of the epitaxial film bulk, other methods (e.g., the Hall method) are better suited.

CONCLUSIONS

In a wide range of conditions, the effect of As^+ ion implantation on the admittance of test MIS structures, based on MBE n-HgCdTe with the composition in the operating layer of 0.22 and near-surface graded-gap layers with increased CdTe content, was studied. Using original techniques, the values of a number of important parameters of MIS structures formed on the basis of as-grown and as-implanted samples were found. It was revealed that, for as-implanted samples, the slow state density decreases slightly, which may be associated with the defect system rearrangement in the MBE HgCdTe near-surface layer. After implantation, the donor concentration in the surface layer increased significantly (up to about 10^{17} cm^{-3}), which is associated with the donor effect of radiation defects based on interstitial mercury atoms introduced during implantation. It was established that the differential resistance of the space-charge region in the strong inversion mode increases significantly (about 50–100 times) after implantation, which is associated with a decrease in the generation rate of minority charge carriers in the near-surface MBE HgCdTe layer. This decrease confirms the previously obtained data on the post-implantation appearance of a thin surface layer with low defect density due to the recombination of a part of the radiation defects during the implantation itself. Donor concentration profiles constructed using the technique with a complex form of voltage sweep ("narrow swing" technique) showed that the post-implantation concentration of donor centers increases with the distance from the interface up to a depth of 90 nm. A slight increase in the conductivity of the MBE HgCdTe film bulk after implantation was noted, but, for detailed studies of changes in the bulk properties of the material, it is preferable to use the Hall method. Good informational content of MIS measurements was shown in studies of the effect of ion implantation on the properties of the near-surface layer of MBE HgCdTe.

ACKNOWLEDGMENTS

This research was supported by Ministry of Science and Higher Education of the Russian Federation, Project No. 0721-2020-0038.

CONFLICT OF INTEREST

The authors declare that they have no conflict of interest.

REFERENCES

1. A. Rogalski, *Infrared and Terahertz Detectors*, 3rd edn (Boca Raton: CRC, 2019).
2. W. Lei, J. Antoszewski, and L. Faraone, *Appl. Phys. Rev.* 2, 041303 (2015).
3. T.J. De Lyon, J.E. Jensen, M.D., Gorwitz, C.A. Cockrum, S.M. Johnson, and G..M. Venzor, *J. Electron. Mater.* 28, 705 (1999).
4. D.D. Edwall, J.S. Chen, J. Bajaj, and E.R. Gertner, *Semicond. Sci. Technol.* 5, S221 (1990).
5. M.B. Reine and M.B. Reine, *Proc. SPIE* 4288, 266 (2001).
6. L. Mollard, G. Bourgeois, C. Lobre, S. Gout, S. Viollet-Bosson, N. Baier, G. Destefanis, O. Gravrand, J.P. Barnes, F. Milesi, A. Kerlain, L. Rubaldo, and A. Manissadjian, *J. Electron. Mater.* 43, 802 (2014).
7. A. Kerlain, A. Brunner, D. Sam-Giao, N. Pére-Laperne, L. Rubaldo, V. Destefanis, F. Rochette, and C. Cervera, *J. Electron. Mater.* 45, 4557 (2016).
8. W. Qiu, W. Hu, C. Lin, X. Chen, and W. Lu, *Opt. Lett.* 41, 828 (2016).
9. L. Mollard, G. Destefanis, N. Baier, J. Rothman, P. Ballet, J.P. Zanatta, M. Tchagaspanian, A.M. Papon, G. Bourgeois, J.P. Barnes, C. Pautet, and P. Fougères, *J. Electron. Mater.* 38, 1805 (2009).
10. L.O. Bubulac, D.S. Lo, W.E. Tennant, D.D. Edwall, J.C. Chen, J. Ratusnik, J.C. Robinson, and G. Bostrup, *Appl. Phys. Lett.* 50, 1586 (1987).
11. L.O. Bubulac, and C.R. Viswanathan, *J. Cryst. Growth* 123, 555 (1992).
12. I.I. Izhnin, A.V. Voitsekhovsky, A.G. Korotaev, O.I. Fitsych, A.Y. Bonchyk, H.V. Savytskyy, K.D. Mynbaev, V.S. Varavin,

S.A. Dvoretsky, N.N. Mikhailov, M.V. Yakushev, and R. Jakiela, *Infrared Phys. Technol.* 81, 52 (2017).
13. C. Lobre, D. Jalabert, I. Vickridge, E. Briand, D. Benzeggouta, L. Mollard, P. H. Jouneau, and P. Ballet, *Nucl. Instrum. Methods Phys. Res. Sect. B* 313, 76 (2013).
14. C. Lobre, P.H. Jouneau, L. Mollard, and P. Ballet, *J. Electron. Mater.* 43, 2908 (2014).
15. A.G.. Korotaev, I.I. Izhnin, K.D. Mynbaev, A.V. Voitsekhovskii, S.N. Nesmelov, S.M. Dzyadukh, O.I. Fitsych, V.S. Varavin, S.A. Dvoretsky. N.N. Mikhailov, M.V. Yakushev, O.Yu. Bonchyk, H.V. Savytsky. Z. Swiatek, J. Morgiel, and M.V. Yakushev, *Surf. Coat. Technol.* 393, 125721 (2020).
16. O.Y. Bonchyk, H.V. Savytskyy, Z. Swiatek, Y. Morgiel, I.I. Izhnin, A.V. Voitsekhovskii, A.G. Korotaev, K.D. Mynbaev, O.I. Fitsych, V.S. Varavin, S.A. Dvoretsky, D.V. Marin, and M.V. Yakushev, *Appl. Nanosci.* 9, 725 (2019).
17. C. Shi, C. Lin, Y. Wei, and L. Chen, *Proc. SPIE* 10177, 101771C (2017).
18. H.R. Vydyanath, and C.H. Hiner, *J. Appl. Phys.* 65, 3080 (1989).
19. H.R. Vydyanath, *J. Vac. Sci. Technol. B: Microelectron. Nanometer Struct. – Process., Meas., Phenom* 9, 1716 (1991).
20. H.R. Vydyanath and H.R. Vydyanath, *J. Cryst Growth* 161, 64 (1996).
21. S.A. Dvoretsky, V.S. Varavin, N.N. Mikhailov, Y.G. Sidorov, T.I. Zakharyash, V.V. Vasiliev, V.N. Ovsyuk, G.V. Chekanova, M.S. Nikitin, IYu. Lartsev, and A.L. Aseev, *Proc. SPIE* 5964, 9640A (2005).
22. E.H. Nicollian, and J.R. Brews, *MOS Physics and Technology* (New York: Wiley, 1982).
23. S. Hlali, A. Farji, N. Hizem, L. Militaru, A. Kalboussi, and A. Souifi, *J. Alloys Compd.* 713, 194 (2017).
24. A.V. Voitsekhovskii, S.N. Nesmelov, S.M. Dzyadukh, V.S. Varavin, S.A. Dvoretsky, N.N., Mikhailov, G.Yu. Sidorov, M.V. Yakushev, and D.V. Marin, *J. Electron. Mater.* 49, 3202 (2020).
25. I.I. Izhnin, K.D. Mynbaev, A.V. Voitsekhovskii, S.N. Nesmelov, S.M. Dzyadukh, A.G. Korotaev, V.S. Varavin, S.A. Dvoretsky, D.V. Marin, M.V. Yakushev, Z. Swiatek, J. Morgiel, and O.Yu. Bonchyk, *Semicond. Sci. Technol.* 35, 115019 (2020). https://doi.org/10.1088/1361-6641/ab924e.
26. A.G. Korotaev, A.V. Voitsekhovskii, I.I. Izhnin, K.D. Mynbaev, S.N. Nesmelov, S.M. Dzyadukh, V.S. Varavin, S.A. Dvoretsky, N.N. Mikhailov, M.V. Yakushev, and GYu. Sidorov, *Surf. Coat. Technol.* 392, 125760 (2020).
27. A.V. Voitsekhovskii, S.N. Nesmelov, and S.M. Dzyadukh, *J. Electron. Mater.* 47, 2694 (2018).
28. A.V. Voitsekhovskii, S.N. Nesmelov, and S.M. Dzyadukh, *J. Phys. Chem. Sol.* 102, 42 (2017).
29. A.V. Voitsekhovskii, S.N. Nesmelov, S.M. Dzyadukh, V.S. Varavin, S.A. Dvoretsky, N.N. Mikhailov, M.V. Yakushev, and G.Y. Sidorov, *Vacuum* 158, 136 (2018).
30. Y.G. Sidorov, S.A. Dvoretskii, V.S. Varavin, N.N. Mikhailov, M.V. Yakushev, and I.V. Sabinina, *Semiconductors* 35, 1045 (2001).
31. R. Fu, J. Pattison, A. Chen, and O. Nayfeh, *Proc. SPIE* 8353, 83532I (2012).
32. P. Zhang, Z.-H. Ye, C.-H. Sun, Y.-Y. Chen, T.-N. Zhang, X. Chen, C. Lin, R.-J. Ding, and L. He, *J. Electron. Mater.* 45, 4716 (2016).
33. E.R. Zakirov, V.G. Kesler, G.Y. Sidorov, I.P. Prosvirin, A.K., Gutakovsky, and V.I. Vdovin, *Semicond. Sci. Technol.* 34, 065007 (2019).
34. E.R. Zakirov, V.G. Kesler, GYu. Sidorov, and A.P. Kovchavtsev, *Semicond. Sci. Technol.* 35, 025019 (2020).
35. A.V. Voitsekhovkii, S.N. Nesmelov, and S.M. Dzyadukh, *Russ. Phys. J.* 52, 1003 (2009).
36. A.V. Voitsekhovkii, S.N. Nesmelov, and S.M. Dzyadukh, *Opto-Electron. Rev.* 22, 236 (2014).
37. A.V. Voitsekhovkii, S.N. Nesmelov, and S.M. Dzyadukh, *Russ. Phys. J.* 48, 584 (2005).
38. A.V. Voitsekhovkii, N.A. Kulchitsky, S.N. Nesmelov, and S.M. Dzyadukh, *J. Comm. Technol. Electron.* 63, 1112 (2018).
39. A.V. Voitsekhovskii, S.N. Nesmelov, S.M. Dzyadukh, V.V. Vasilev, V.S. Varavin, S.A. Dvoretsky, N.N. Mikhailov, M.V. Yakushev, and G.Y. Sidorov, , *Phys. Stat. Sol. (c)* 13, 647 (2016).
40. A.P. Kovchavtsev, G.Y. Sidorov, A.E. Nastovjak, A.V. Tsarenko, I.V. Sabinina, and V.V. Vasilyev, *J. Appl. Phys.* 121, 125304 (2017).
41. S.M. Sze, and K.K. Ng, *Physics of Semiconductor Devices*, 3rd edn (New Jersey: Wiley, 2007).
42. W. Van Gelder, and E.H. Nicollian, *J. Electrochem. Soc.* 118, 138 (1971).
43. T. Nakagawa, and H. Fujisada, *Appl. Phys. Lett.* 31, 348 (1977).
44. I.I. Izhnin, I.I. Syvorotka, O.I. Fitsych, V.S. Varavin, S.A. Dvoretsky, D.V. Marin, N.N. Mikhailov, V.G. Remesnik, M.V. Yakushev, K.D. Mynbaev, A.V. Voitsekhovsky, and A.G. Korotaev, *Semicond. Sci. Technol.* 34, 035009 (2019).
45. G.A. Umana-Membreno, H. Kala, J. Antoszewski, Z.H. Ye, W.D. Hu, R.J. Ding, X.S. Chen, W. Lu, L. He, J.M. Dell, and L. Faraone, *J. Electron. Mater.* 42, 3108 (2013).
46. J.R. Brews and J.R. Brews, *J. Appl. Phys.* 44, 3228 (1973).
47. O.Yu. Bonchyk, H.V. Savytskyy, I.I. Izhnin, K.D. Mynbaev, I.I. Syvorotka, A.G. Korotaev, A.V. Voitsekhovskii, O.I. Fitsych, V.S. Varavin, D.V. Marin, N.N. Mikhailov, M.V. Yakushev, Z. Swiatek, J. Morgiel, and R. Jakiela, *Appl. Nanosci.* **10**, 4971 (2020). https://doi.org/10.1007/s13204-020-01327-9.

Publisher's Note Springer Nature remains neutral with regard to jurisdictional claims in published maps and institutional affiliations.